OPEN ACCESS
CellPress

Cell Reports
Report

HDAC6 Is a Bruchpilot Deacetylase that Facilitates Neurotransmitter Release

Katarzyna Miskiewicz,[1,2,7] Liya E. Jose,[1,2,7] Wondwossen M. Yeshaw,[1,2,8] Jorge S. Valadas,[1,2] Jef Swerts,[1,2] Sebastian Munck,[1,2,3] Fabian Feiguin,[4] Bart Dermaut,[5,6] and Patrik Verstreken[1,2,*]

[1]VIB Center for the Biology of Disease, Herestraat 49 bus 602, 3000 Leuven, Belgium
[2]KU Leuven, Center for Human Genetics and Leuven Research Institute for Neuroscience and Disease (LIND), Herestraat 49 bus 602, 3000 Leuven, Belgium
[3]VIB Bio Imaging Core, Herestraat 49 bus 602, 3000 Leuven, Belgium
[4]International Center for Genetic Engineering and Biotechnology, Padriciano 99, 34149 Trieste, Italy
[5]INSERM U744, Institut Pasteur de Lille, Université de Lille Nord de France, rue du Professeur Calmette 1, 59019 Lille, France
[6]Center for Medical Genetics, Ghent University Hospital, De Pintelaan 185, 9000 Gent, Belgium
[7]Co-first author
[8]Present address: Department of Cell Biology, University Medical Center Groningen, University of Groningen, A. Deusinglaan 1, 9713 AV Groningen, the Netherlands
*Correspondence: patrik.verstreken@cme.vib-kuleuven.be
http://dx.doi.org/10.1016/j.celrep.2014.05.051

SUMMARY

Presynaptic densities are specialized structures involved in synaptic vesicle tethering and neurotransmission; however, the mechanisms regulating their function remain understudied. In *Drosophila*, Bruchpilot is a major constituent of the presynaptic density that tethers vesicles. Here, we show that HDAC6 is necessary and sufficient for deacetylation of Bruchpilot. HDAC6 expression is also controlled by TDP-43, an RNA-binding protein deregulated in amyotrophic lateral sclerosis (ALS). Animals expressing TDP-43 harboring pathogenic mutations show increased HDAC6 expression, decreased Bruchpilot acetylation, larger vesicle-tethering sites, and increased neurotransmission, defects similar to those seen upon expression of HDAC6 and opposite to hdac6 null mutants. Consequently, reduced levels of HDAC6 or increased levels of ELP3, a Bruchpilot acetyltransferase, rescue the presynaptic density defects in TDP-43-expressing flies as well as the decreased adult locomotion. Our work identifies HDAC6 as a Bruchpilot deacetylase and indicates that regulating acetylation of a presynaptic release-site protein is critical for maintaining normal neurotransmission.

INTRODUCTION

Synaptic vesicles fuse with the plasma membrane at presynaptic release sites. While SNAREs (soluble NSF attachment receptors) are essential for fusion, the neurotransmitter release process is modulated by numerous additional mechanisms. The presynaptic dense body is an evolutionary conserved structure that is involved in capturing and concentrating synaptic vesicles at release sites (Hallermann et al., 2010a; Mukherjee et al., 2010). In fruit flies, a major constituent of this structure is the cytoskeletal-like protein Bruchpilot (BRP) (Wagh et al., 2006). Although the presynaptic dense body and BRP are critical to maintain normal levels of synaptic transmission, the mechanisms that regulate the function of this structure remain largely unknown.

The BRP protein organizes in parallel strands with their N termini facing the plasma membrane while sending their C termini into cytoplasm to contact and tether synaptic vesicles (Fouquet et al., 2009). BRP is acetylated by the synaptic acetyl transferase (HAT) ELP3 (Miśkiewicz et al., 2011), and lysine acetylation is believed to neutralize positive charges at the BRP C-terminal end, thus regulating dense body (T-bar) morphology and function. If acetylation is a regulatory mechanism to modify BRP, it should be reversible; however, the BRP deacetylase is not known.

Here, we report that the cytoplasmic deacetylase HDAC6 is necessary and sufficient for BRP deacetylation. Deacetylation of BRP in animals that overexpress HDAC6 results in larger T-bars that contact more synaptic vesicles resulting in a larger readily releasable vesicle pool, while *hdac6* null mutants show the opposite phenotype. Interestingly, HDAC6 is a target of the RNA-binding protein TDP-43 that is mutated in amyotrophic lateral sclerosis (ALS), and both the loss and gain of TDP-43 function phenocopy the loss and gain of HDAC6, respectively. Providing further functional relevance, genetically upregulating BRP acetylation by downregulating HDAC6 or upregulating ELP3 in TDP-43-expressing flies can rescue the synaptic and locomotion defects observed in these animals. Hence, our work in fruit flies suggests that BRP acetylation is under the control of two intersecting pathways: Elp3-dependent acetylation and HDAC6-dependent deacetylation.

RESULTS

HDAC6 Promotes the Formation of Larger T-Bars with More Tethered Synaptic Vesicles

HDAC6 is a cytoplasmic deacetylase expressed in neurons (Fukada et al., 2012). To explore synaptic defects associated

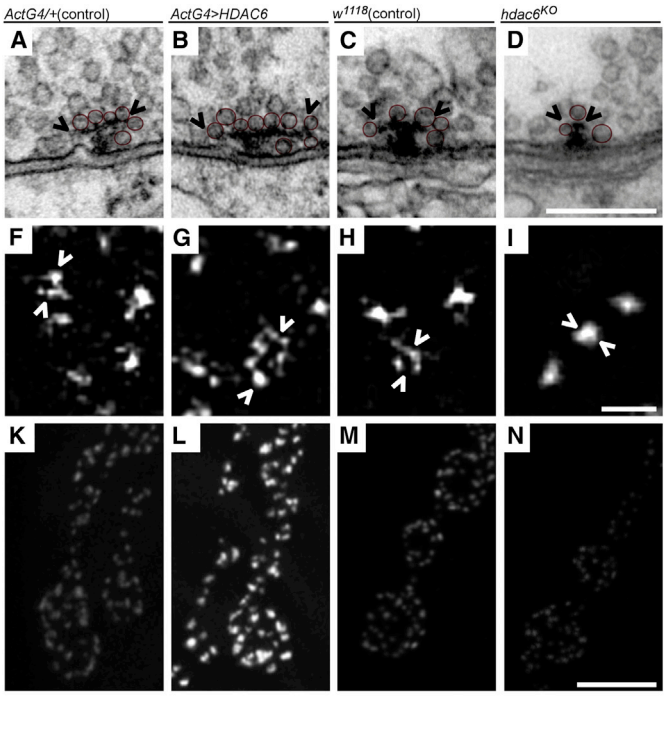

Figure 1. Gain or Loss of HDAC6 Function Results in Morphological Defects at the T-Bar Top

(A–E) TEM micrographs of T-bars (A–D) in controls (A, *ActGAL4*/+ or C, w^{1118}), in animals overexpressing *Drosophila* HDAC6 (B, *P[UAShdac6]*/+; *ActGAL4*/+), and in *hdac6* null mutants (D, $hdac6^{ko}$); and quantification of T-bar platform length (E and arrowheads in A–D) and the percent T-bars with a platform larger than 200 nm (numbers in E). Tethered vesicles are encircled and quantified in (P). n = 50–215 from more than three animals. Box, interquartile range; horizontal line, mean; vertical line, range. t test: *p < 0.05, **p < 0.01. Scale bar in (D), 0.25 μm.

(F–J) PiMP of BRP^C labeling (F–I) and quantification of BRP^C-ring surface area (J) and arrowheads in (F)–(I). n = 153–371 BRP dots from at least five animals. Box plot as in (E) and normalized to controls. t test: ***p < 0.001. Scale bar in (I), 0.5 μm.

(K–O) Confocal images (K–N) of boutons labeled with BRP^C and quantification of labeling intensity (O); n = 6–10 NMJs collected from five animals. Data are normalized to controls. Error bars represent SEM. t test: **p < 0.01. Scale bar in (N), 5 μm.

(P) Quantification of the number of vesicles tethered to T-bars in electron micrographs (P) and indicated in (A)–(D). n = 53–117 from more than three animals. t test: ***p < 0.001.

See also Figure S1.

with altered levels of HDAC6, we used $hdac6^{ko}$ null mutants and overexpression of *hdac6* (Figure S1A) and assessed presynaptic morphology at the *Drosophila* larval neuromuscular junction using transmission electron microscopy (TEM). We find that many synaptic features, including the number of T-bars, synaptic vesicles, or mitochondria per boutonic area, are not different from controls (Figures S1B–S1H), indicating proper delivery of these components to synaptic boutons. However, using serial-section electron microscopy, in $hdac6^{ko}$ animals we do observe T-bars with significantly smaller "top sizes." Conversely, animals overexpressing HDAC6 show T-bars with larger top sizes when compared to controls (Figures 1A–1E). Hence, HDAC6 regulates T-bar morphology.

Next, we applied superresolution photobleaching microscopy with nonlinear processing (PiMP) imaging (Munck et al., 2012) using BRP^C antibodies that recognize the BRP C-terminal end and label the T-bar top (Fouquet et al., 2009). BRP^C dots are diffraction limited, but PiMP reveals BRP^C rings that label the T-bar top edge. Corroborating our TEM results, in animals overexpressing HDAC6, the average size of these BRP^C rings is substantially increased (Figures 1F, 1G, and 1J), while in $hdac6^{ko}$ mutants, BRP^C rings are smaller compared to controls (Figures 1H–1J). These changes at the T-bar top also result in altered BRP^C immunoreactivity levels, likely as a result of differences in antibody accessibility; in $hdac6^{ko}$ synapses, we observe a decrease in BRP^C labeling intensity, and overexpression of HDAC6 causes an increase in BRP^C labeling (Figures 1K–1O). Labeling with a BRP^N antibody that recognizes the BRP N terminus facing the plasma membrane does not show a difference in labeling intensity (not shown), indicating the assembly of BRP strands in T-bars is not disrupted. Taken together, the data indicate HDAC6 promotes the reorganization of the BRP C terminus to form larger T-bar tops.

Presynaptic T-bars coordinate neurotransmission by facilitating vesicle tethering (Hallermann et al., 2010a). We therefore quantified the number of T-bar-tethered vesicles. Animals that overexpress HDAC6 show an increased number of tethered vesicles, while $hdac6^{ko}$ mutants harbor less tethered synaptic vesicles compared to controls (Figure 1P). Hence, in contrast to *hdac6* loss of function, the overexpression of HDAC6 causes T-bar tops to expand, enabling them to contact more synaptic vesicles.

HDAC6 Results in a Larger Readily Releasable Vesicle Pool

To assess if changes in T-bar morphology and the number of tethered vesicles correlate with defects in neuronal function, we resorted to electrophysiology. First, we recorded neurotransmission in hemolymph-like physiological solution (HL-3) with 0.45 mM $CaCl_2$ to reveal exocytic defects. At low-frequency stimulation, the excitatory junctional current (EJC) amplitude in *hdac6* mutants is marginally smaller. Conversely, EJC amplitudes are significantly increased when HDAC6 is overexpressed (Figure 2A). Given that the mean miniature EJC amplitude is not significantly affected (Figure 2B), the quantal content upon overexpression of HDAC6 is increased (Figure 2C). To find a functional correlate for the alterations in T-bar-tethered vesicles, we next assessed the size of the pool of synaptic vesicles that can be released during a very short bout of intense stimulation (1 s, 60 Hz). We performed this experiment in 5 mM $CaCl_2$,

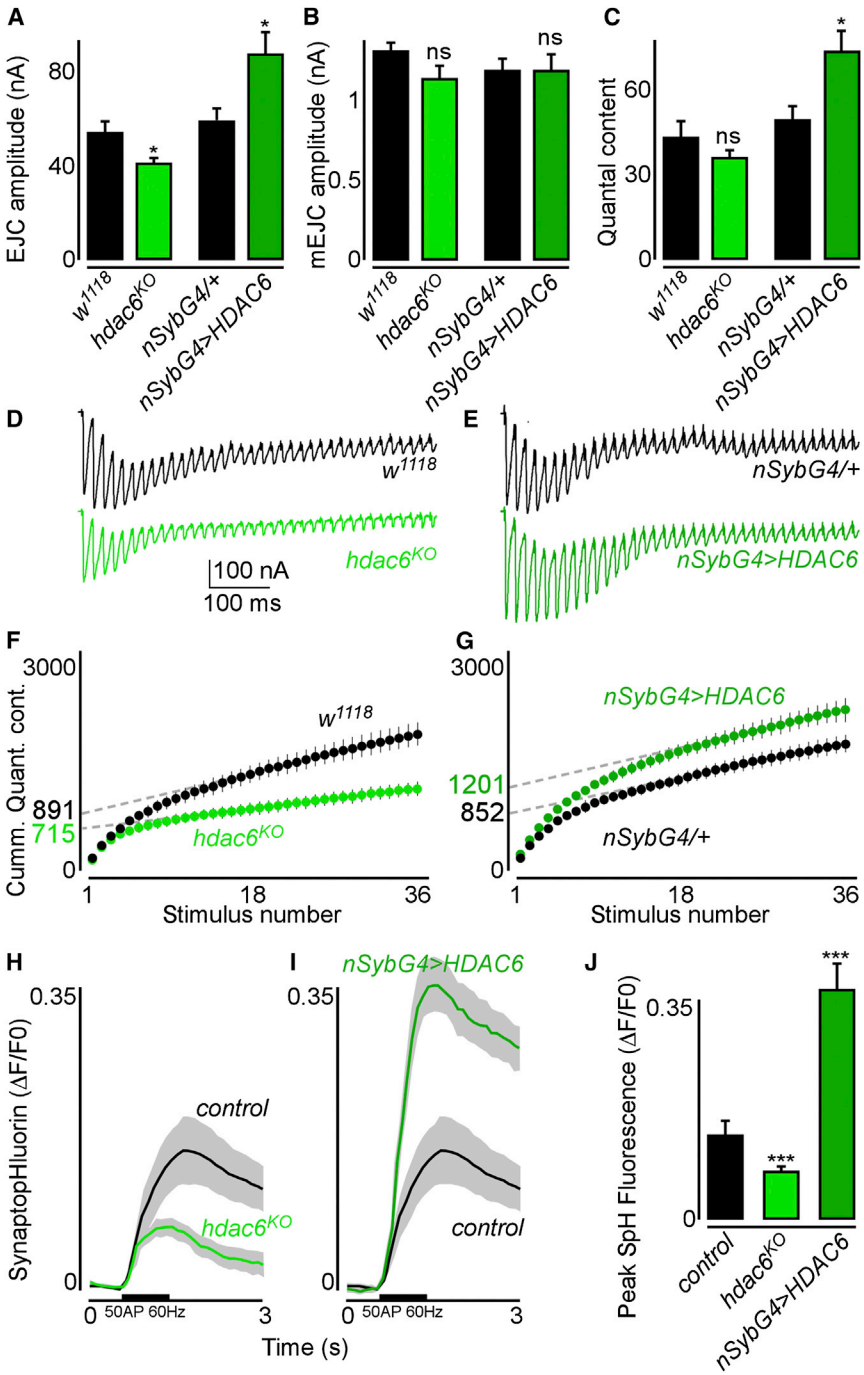

Figure 2. HDAC6 Promotes the Formation of the Readily Releasable Vesicle Pool

(A–C) Quantification of EJC (A) and miniature EJC (mEJC) (B) amplitude measured in HL-3 with 0.45 mM $CaCl_2$ (and TTX for minis), and the quantal content (EJC/mean mEJC) (C) in the genotypes listed in Figure 1, except HDAC6 was overexpressed using *nSybGAL4* and the control is *nSybGal4/+*. n > 10. Error bars represent SEM. t test: *p < 0.05; ns, not significant.

(D–G) Raw data traces of EJC recordings made in 5 mM calcium at 60 Hz in w^{1118} (black in D) and *nSybGal4/+* controls (black in E) in $hdac6^{KO}$ mutants (light green, D) and in animals overexpressing HDAC6 (dark green, E) and quantification of the cumulative released quantal content in such recordings versus stimulus number. The y-intercept of the slope of the trend line (dotted line) at steady state (points 24–36) provides a measure of the average RRP size (indicated on the y axis). n > 9. Error bars represent SEM.

(H–J) Releasable vesicle fusion measured as the mean relative synaptopHluorin (SpH) fluorescence change (ΔF/Fo) during a 60 Hz 50 action potential train (black line). The average ΔF/Fo plotted as a function of time and the SEM in gray (H and I) as well as the maximum ΔF/Fo (J). Control: *nsybGal4/UAS-SpH*. n = 6–12 animals. Error bars represent SEM. ANOVA/Dunnett: ***p < 0.001.

ensuring an invariable high release probability. During the first stimulations, this protocol results in the fusion of ready-to-release vesicles (Hallermann et al., 2010b). Back extrapolation of the cumulative quantal content indicates that in *hdac6* mutants 20% (p = 0.05), less vesicles were ready for release than in controls, while in animals overexpressing HDAC6, the size of this vesicle pool is 41% (p < 0.01) increased compared to controls (Figures 2D–2G). To independently measure vesicle fusion during high-frequency stimulation, we resorted to synaptopHluorin (SpH) (Miesenböck et al., 1998). SpH is a pH-sensitive vesicle-associated probe that increases in fluorescence when exposed to the extracellular environment. The SpH signal upon stimulation of motor neurons at 60 Hz (50 stimuli) increases dramatically. However, in *hdac6* mutants, this increase is trumped in comparison to control, while overexpression of HDAC6 results in a larger peak fluorescence level (Figures 2H–2J). Taken together, the morphological and functional data indicate HDAC6 is a positive regulator of a larger ready-to-release pool of synaptic vesicles.

HDAC6 Is Necessary and Sufficient to Deacetylate BRP

Reduced BRP acetylation levels at fly neuromuscular junctions (NMJs) result in T-bars with larger top sizes and increased neurotransmitter release (Miśkiewicz et al., 2011), phenotypes very reminiscent of those we observe in animals overexpressing HDAC6. We therefore tested the hypothesis that HDAC6 mediates BRP deacetylation in vivo. We immunoprecipitated BRP from heads of controls, $hdac6^{ko}$ flies, and flies overexpressing HDAC6 and probed western blots with antibodies recognizing acetylated lysines (ac-K). Compared to controls, we observed a stronger ac-K band that migrates at the height of BRP in $hdac6^{ko}$ mutants and a weaker ac-K band in BRP immunoprecipitates

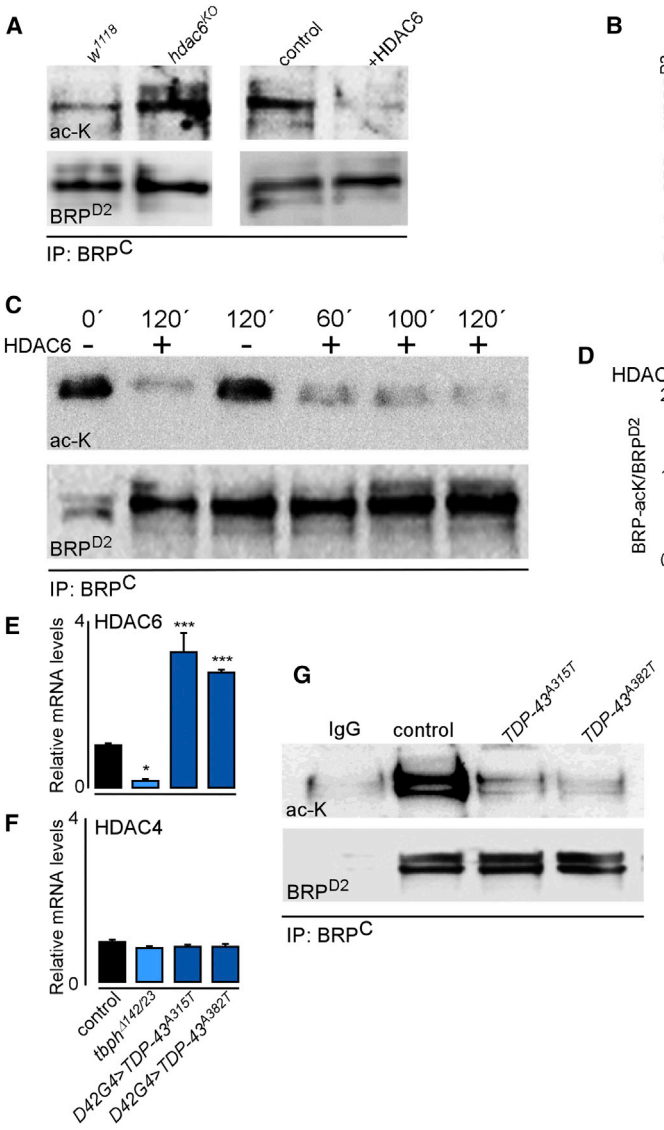

Figure 3. HDAC6 Is a BRP Deacetylase Whose Expression Is Increased in TDP-43 Pathogenic Mutant-Expressing Animals

(A and B) Western blots probed with anti-ac-K and BRP^{D2} of immunoprecipitated (IP) BRP from controls (w^{1118} and *Act-Gal4*), $hdac6^{ko}$ null mutants, and animals overexpressing HDAC6 (A), and quantification of ac-K intensity normalized to BRP^{D2} and relative to the respective controls (B).

(C and D) Western blots of time-dependent in vitro deacetylation of immunoprecipitated BRP (using BRP^{C}) from w^{1118} fly heads using recombinant HDAC6. ac-K (C), and quantification of ac-K intensity (D).

(E and F) mRNA levels of HDAC6 (E) and HDAC4 (F), relative to *RP49*, normalized to controls (w^{1118} or *D42Gal4*/+).

(G and H) Western blot probed for ac-K of immunoprecipitated BRP from controls (*ElavGAL4*/+) and of animals expressing $TDP\text{-}43^{A315T}$ or $TDP\text{-}43^{A382T}$ (G), and quantification of ac-K intensity (H). Error bars represent SEM ANOVA/Dunnett: ***$p < 0.001$.

See also Figure S2.

from animals overexpressing HDAC6 (Figures 3A and 3B). Hence, HDAC6 is necessary to promote BRP deacetylation in vivo. To test if HDAC6 can deacetylate BRP directly, we immunoprecipitated BRP from wild-type fly heads and incubated these BRP-enriched fractions with recombinant HDAC6. Probing western blots for ac-K shows a time-dependent deacetylation of BRP by HDAC6 (Figures 3C and 3D). Thus, HDAC6 is also sufficient for BRP deacetylation in vitro.

The RNA-Binding Protein TDP-43 Regulates HDAC6 Expression and Induces T-Bar Morphology Defects

To independently manipulate HDAC6 levels and assess T-bar morphology, we resorted to TDP-43, an RNA-binding protein that is found in a complex with *HDAC6* mRNA and regulates HDAC6 expression (Kim et al., 2010). Flies mutant for *tbph,* the TDP-43 homolog, show reduced *HDAC6* mRNA levels (Fiesel et al., 2010), indicating HDAC6 expression is regulated by TDP-43. Using quantitative RT-PCR, we confirm the reduced *HDAC6* mRNA levels in *tbph* mutants, and we also find an upregulation of *HDAC6* mRNA in animals overexpressing wild-type human TDP-43 (*nSyb-Gal4*, $p < 0.001$; *D42-Gal4*, $p = 0.05$; Figure S2A) or TDP-43 harboring mutations that cause ALS in patients ($TDP43^{A315T}$ or $TDP\text{-}43^{A382T}$; *nSyb-Gal4,* $p < 0.001$ not shown; *D42-Gal4*, $p < 0.001$; Figure 3E). Indicating specificity, the expression of HDAC4, another cytoplasmic deacetylase not targeted by TDP-43, is not altered (Figure 3F). Expression of $TDP43^{A315T}$ and $TDP\text{-}43^{A382T}$ yield a more robust increase in HDAC6 expression compared to TDP-43, and we therefore tested if expression of $TDP43^{A315T}$ and $TDP\text{-}43^{A382T}$ would reduce BRP acetylation levels by immunoprecipitating BRP and probing the western blots using anti-ac-K. As shown in Figures 3G and 3H, we observe a much weaker ac-K band in TDP-43 mutant-expressing animals. The developmental lethality associated with *tbph* null mutations precluded us from examining BRP acetylation in the heads of these animals. Nonetheless, our data indicate that BRP is deacetylated in animals that express mutant TDP-43, a defect that correlates with upregulated HDAC6 expression levels.

TDP43- and HDAC6-Induced T-Bar Defects Are Similar

If HDAC6 regulates T-bar morphology in a dosage-sensitive manner, we expect altered TDP-43 function to also show structural defects at the level of T-bars. We therefore overexpressed TDP-43 using neuronal drivers of different strength and found that the intensity of BRP^{C} immunolabeling relates in

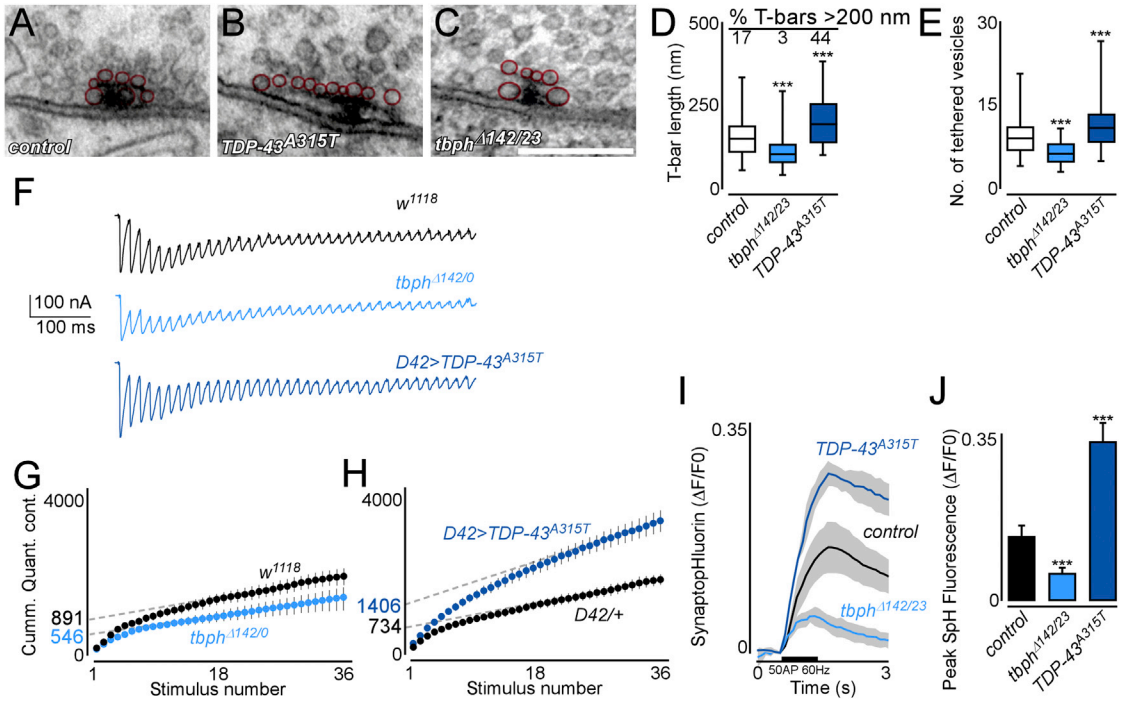

Figure 4. Increased HDAC6 Levels upon TDP-43 Expression Correlate with Increased Synaptic Vesicle Tethering

(A–C) TEM micrographs of T-bars at boutons of controls (A, *D42*/+), *TDP-43*^{A315T}-expressing animals (B), and *tbph*$^{\Delta142/23}$ mutants (C) highlighting the T-bar-tethered vesicles. *w*^{1118} controls and *TDP-43*^{A382T} mutants are not shown but yield very similar results to *D42*/+ and *TDP-43*^{A315T}, respectively. Scale bar in (C) for (A)–(C) represents 0.25 μm.

(D and E) Quantification of the T-bar platform length (D), the percent of T-bars with a platform larger than 200 nm (numbers in D), and the number of tethered vesicles (E). In (D), n = 402–493 T-bars; in (E), n = 33–219, from at least animals. *TDP-43*^{A382T} mutant is not shown but yields very similar results to *TDP-43*^{A315T}. Box: as in Figure 1. ANOVA/Kruskal-Wallis/Dunnett/Dunn: ***p < 0.001.

(F–H) Raw data traces of EJC recordings made in HL-3 with 5 mM calcium and stimulated at 60 Hz in *w*^{1118} controls (*D42*/+ controls appear very similar, black) in *tbph*$^{\Delta142/0}$ mutants (light blue) and in animals expressing TDP-43^{A315T} (dark blue, F), and quantification of the cumulative released quantal content in such recordings versus stimulus number. The y-intercept of the slope of the trend line (dotted line) at steady state (points 24–36) provides a measure of the average RRP size (indicated on the y axis). n > 9. Error bars represent SEM.

(I and J) Synaptic vesicle fusion measured as the mean relative synaptopHluorin (SpH) fluorescence change (ΔF/Fo) during a 60 Hz 50 action potential train (black line). The average ΔF/Fo plotted as a function of time and the SEM in gray (I) and the maximum ΔF/Fo (J). *TDP-43*^{A382T} mutant is not shown but yields very similar results to *TDP-43*^{A315T}. n = 5–12 animals. Error bars represent SEM. ANOVA/Dunnett: ***p < 0.001.

See also Figure S3.

a dosage-sensitive manner to the strength of the GAL4 driving TDP-43 expression (*nSyb-Gal4* > *Elav-Gal4* > *D42-Gal4*; Figures S2B–S2D′ and S2G) (Khuong et al., 2010). Similarly, overexpression of TDP-43 pathogenic mutants triggered increased BRP^{C} labeling (Figures S2E–S2G), indicating this defect is the result of a gain-of-function mechanism. Note that under the same conditions, BRP assembly is not affected, because BRP^{N} labeling intensity is not different (data not shown). While expression of wild-type TDP-43 or the pathogenic TDP-43 mutants all cause more intense BRP^{C} labeling compared to controls (Figures S2B–S2G), when expressed at similar levels, the pathogenic mutants cause the strongest increase, again correlating with the level of increase in HDAC6 expression (compare Figure S2D′ to Figures S2E and S2F). One possibility explaining the less severe effects we observe upon expression of wild-type TDP-43 is that wild-type TDP-43 autodownregulates the expression of endogenous TDP-43 (*tbph*), thus compensating for the increased HDAC6 levels (Ayala et al., 2011). Another possibility is that the pathogenic TDP43 proteins localize differently in comparison to the wild-type TDP-43, harboring additional or stronger effects on HDAC6 mRNA (Estes et al., 2011; Kim et al., 2010). The extent to which either of these mechanisms is at play in fly motor neurons needs to be further explored in the future.

Given that the TDP-43 pathogenic mutants already show a strong effect on BRP^{C} labeling when expressed with the weaker *D42-Gal4* driver (Figures S2E–S2G), we used this condition to further study the T-bar defects. First, we used PiMP (Figures S2H–S2N) and TEM (Figures 4A, 4B, and 4D) to assess T-bar top size. We measure larger T-bar top sizes in animals expressing TDP-43 pathogenic mutants, and these T-bars show an increased number of tethered vesicles (Figure 4E). Other synaptic features, including the number of synaptic vesicles, mitochondria, and T-bars, are not different, indicating that these components are properly delivered to the nerve terminals (Figures S3A–S3F). Opposite to animals that express pathogenic TDP-43, *tbph* mutants harbor T-bars with significantly

smaller top sizes (Figures S2K, S2L, and S2N and Figures 4C and 4D), and these T-bars harbor less tethered synaptic vesicles than control T-bars (Figure 4E). Hence, T-bar top size and vesicle tethering are oppositely affected in *tbph* mutants compared to animals expressing TDP-43 pathogenic mutants, and these defects correlate with HDAC6 expression levels (see also below).

To determine if the morphological changes at the T-bar top upon expression of TDP-43 correlate with functional defects, we measured the size of the ready-to-release vesicle pool using two electrode voltage clamps. First, we measured EJCs in 0.45 mM $CaCl_2$ at 0.2 Hz and find the EJC amplitude and quantal content is increased in animals expressing TDP-43^{A315T} mutants, but not affected in *tbph* mutants (Figures S3G–S3J). Next, we measured the number of quanta released during a 60 Hz stimulation paradigm. Back extrapolation of the cumulative quantal content indicates that the ready-to-release vesicle pool compared to controls is 92% ($p < 0.01$) larger in animals expressing TDP-43 pathogenic mutants and 39% ($p = 0.02$) smaller in *tpbh* mutants (Figures 4F–4H). The smaller readily releasable pool we measure in *tbph* mutants seems at odds with the unaffected basal release measured at 0.2 Hz (Figures S3G–S3J). While more work is needed, we surmise that deregulation of additional targets of TBPH may affect EJC amplitudes independent of the effects on the ready-to-release vesicle pool. To further scrutinize vesicle release during intense stimulation, we also used SpH in animals that express pathogenic TDP-43 or in *tbph* mutants and stimulated their motor neurons using 50 stimuli at 60 Hz. We find a significantly higher SpH peak fluorescence level in neurons expressing TDP-43 pathogenic mutants, while *tbph* mutants only show a marginal change in SpH signal (Figures 4I and 4J). Hence, the increased HDAC6 levels in animals expressing TDP-43 pathogenic mutants correlate with more tethered vesicles and an increased size of the readily releasable vesicle pool, while the decreased levels of HDAC6 in *tbph* mutants correlate with less tethered vesicles and a smaller readily releasable vesicle pool.

HDAC6 and ELP3 Genetically Interact to Regulate BRP Acetylation

To scrutinize the in vivo role of HDAC6 as a BRP deacetylase, we performed genetic interaction experiments. We reasoned that either increased levels of ELP3 or reduced levels of HDAC6 would antagonize the defects seen upon expression of TDP-43 pathogenic mutants. First, we assessed BRP acetylation levels. While overexpression of the TDP-43 pathogenic mutants alone leads to a less BRP acetylation (Figures 3G and 3H), co-overexpressing ELP3 or removing one copy of *hdac6* rescues this defect (Figures 5A and 5B). Next, we tested if gain of ELP3 or partial loss of HDAC6 rescues T-bar morphology in flies expressing pathogenic TDP-43 and found, using PiMP, that both these conditions rescue the larger T-bar tops (Figures 5C–5G). Furthermore, increasing ELP3 or decreasing HDAC6 also rescued the excessive vesicle fusion seen upon intense stimulation in TDP-43-expressing animals, as gauged by SpH imaging (Figure 5H). Hence, ELP3 and HDAC6 antagonistically regulate BRP acetylation, T-bar top size, and the size of the pool of vesicles that is ready for fusion during intense stimulation.

Aged flies expressing pathogenic TDP-43 show reduced motor activity in an automated 24 hr monitoring system (Figure 5I) as well as reduced negative geotaxis (Figure 5J) (Voigt et al., 2010; Estes et al., 2011). We wondered if correcting BRP acetylation levels in animals that express pathogenic TDP-43 would correlate with improved motor performance in these animals. While overexpression of ELP3 or heterozygosity for *hdac6* alone has no effect on activity or negative geotaxis (data not shown), these conditions both significantly rescue the activity and geotaxis defects in pathogenic TDP-43-expressing animals (Figures 5I and 5J). These data suggest that excessive BRP deacetylation contributes to TDP43-induced motor defects in flies and that promoting synaptic BRP reacetylation alleviates these disabilities.

DISCUSSION

Here, we find that HDAC6 controls vesicle tethering and synaptic transmission by regulating BRP deacetylation, thereby antagonizing ELP3, a BRP acetyltransferase (Miśkiewicz et al., 2011). Our work defines BRP as a deacetylation target of HDAC6. Acetylation of the C-terminal end of BRP results in more condensed T-bars, while deacetylation leads the protein to send excessive tentacles into the cytoplasm to contact more synaptic vesicles. Similar to chromatin structure being regulated by electrostatic mechanisms at the level of histone acetylation, we propose that electrostatic interactions between acetylated and deacetylated lysines in individual BRP strands regulate presynaptic density structure and function.

While many HDAC-like proteins are present in the nucleus to deacetylate histones, HDAC6 predominantly locates to the cytoplasm, where it has been implicated in the modification of different proteins, including α-tubulin, contractin, and HSP90 (Hubbert et al., 2002; Kovacs et al., 2005; Zhang et al., 2007). In neurons, HDAC6-dependent α-tubulin deacetylation may affect axonal transport by promoting kinesin-1 and dynein binding to microtubules (Reed et al., 2006). However, *hdac6* null mutant flies did not show overt changes in synaptic features other than T-bar morphology as gauged by electron microscopy, suggesting that axonal transport as a consequence of tubulin defects was not massively affected, although we do not exclude more subtle transport defects.

BRP is a presynaptic density structural component important to cluster calcium channels at release sites while tethering synaptic vesicles at its C-terminal end (Kittel et al., 2006; Wagh et al., 2006). The regulation of BRP by HDAC6-dependent deacetylation indicates the BRP C-terminal end is important to sustain neurotransmitter release during intense (60 Hz) stimulation by orchestrating vesicle tethering. Corroborating these results, mutations in the BRP C-terminal end (brp^{nude}) cause defects in vesicle tethering and the maintenance of release during intense 60 Hz stimulation (Hallermann et al., 2010a). Similarly *brp*-isoform mutations that leave calcium channel clustering intact but result in a much more condensed T-bar top show a smaller readily releasable vesicle pool (Matkovic et al., 2013), very similar to the defects we observe when BRP is excessively acetylated (this study and Miśkiewicz et al., 2011). The brp^{nude} mutation shows somewhat less severe defects to maintain synaptic transmission, possibly because more vesicles still manage to tether in

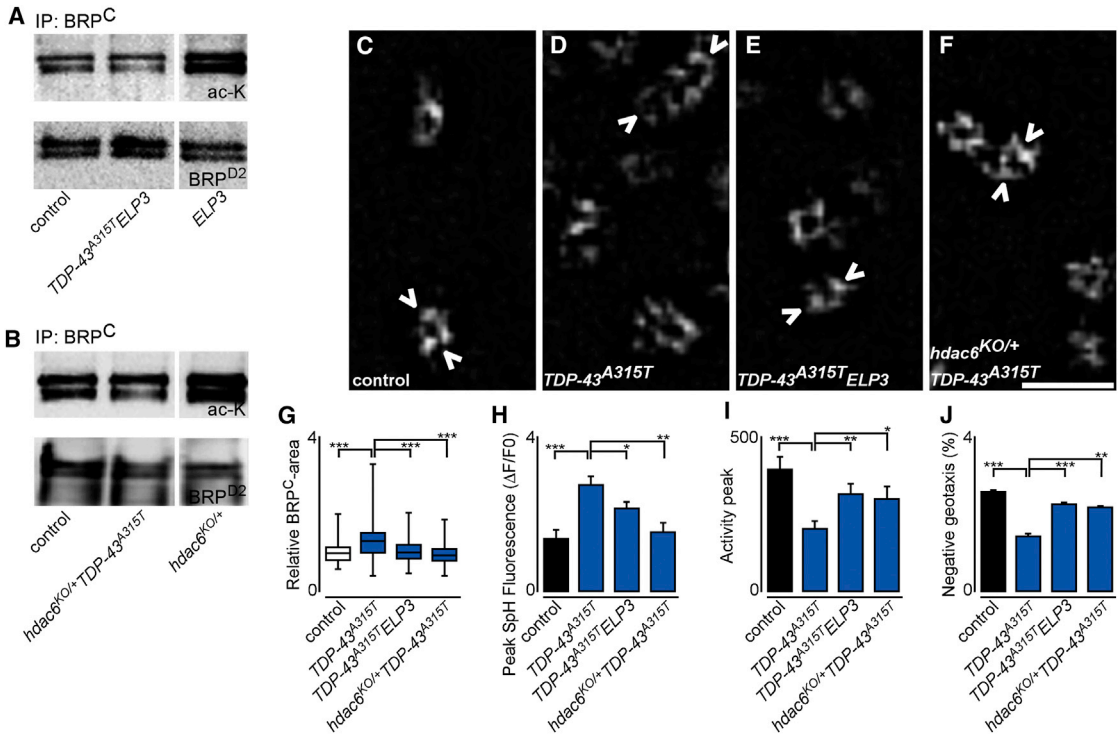

Figure 5. Genetic Interactions between HDAC6 and Elp3 Regulate BRP Acetylation and Rescue Defects in TDP-43 Pathogenic Mutant-Expressing Animals

(A and B) Western blots of immunoprecipitated BRP probed with ac-K and with BRP^{D2}. Control (*ElavGAL4*/+) (lane 1 in A and B); animals expressing *TDP-43*^{A315T} and hELP3 (using *ElavGAL4*) (lane 2 in A) or heterozygous for *hdac6*^{ko} (lane 2 in B); animals overexpressing hELP3 (*ElavGAL4; UAShELP3*/+) (lane 3 in A) or heterozygous for *hdac6*^{ko} (lane 3 in B). Compare to Figure 3G, lane 3.

(C–G) PiMP images (C–F) and quantification of BRP^{C}-ring surface area. n = 138–347 from five animals. Data normalized to controls. Box plots as in Figure 1. ANOVA/Dunnett: ***p < 0.001. Scale bar, 0.5 μm.

(H) Synaptic vesicle fusion measured as the mean relative SpH fluorescence change (ΔF/Fo) during a 60 Hz 50 action potential train and quantification of maximum ΔF/Fo. The data in bar 2 are identical to the data in bar 3 in Figure 4G. n = 5–12 animals. ANOVA/Dunnett: ***p < 0.001.

(I and J) Morning peak activity levels (I) in a 24 hr activity monitor and negative geotaxis (J). Error bars represent SEM. n = 20 (A); n = 4 (B). ANOVA/Kruskal-Wallis in (I) Dunnett/Dunn in (J): ***p < 0.001; **p < 0.01; *p < 0.05.

In (G) –(I), the difference between control and the conditions that rescue *TDP-43*^{A315T} is not significant (not shown).

these mutants during stimulation compared to the conditions that result in strong shrinking of the T-bar top. Nonetheless, the data indicate that in flies, BRP orchestrates efficient synaptic transmission during intense activity.

In the model we present, ELP3 and HDAC6 antagonistically control presynaptic function. TDP-43, a gene mutated in ALS, positively regulates HDAC6 expression, and in flies, increased HDAC6 activity or expression of pathogenic TDP-43 results in the deacetylation of active zone material and increased synaptic release. Remarkably, the presence of an ALS risk-associated *ELP3* allele in humans correlates with reduced ELP3 expression in ALS patient spinal cords (Simpson et al., 2009). In flies, *elp3* mutants also cause active zone deacetylation and more synaptic release. Together with genetic interactions in fruit flies, the data suggest that decreased HDAC6 function and increased ELP3 function act antagonistically, both in flies and humans. However, the target(s) on which these enzymes converge in humans remains to be discovered. In flies, our data are consistent with ELP3-dependent acetylation to occur at the C-terminal tail of the BRP protein (this work and Miśkiewicz et al., 2011). However, the mammalian BRP counterpart, ELKS/CAST, that resides in the presynaptic density (Ohtsuka et al., 2002), does not contain a long C-terminal tail (Wagh et al., 2006). ELKS/CAST in mammals has been found to be associated with filamentous structures (Siksou et al., 2007), and the activity to concentrate synaptic vesicles near release sites may thus be executed by binding partners of ELKS/CAST such as Picollo or Bassoon (Mukherjee et al., 2010). Hence, it will be interesting to test if ELP3 and HDAC6 regulate acetylation at the much shorter ELKS/CAST tail or whether ELKS/CAST binding partners are acetylated also in the context of ALS. It is in this perspective interesting to note that another active zone-associated protein, UNC13A, is implicated in ALS as well (Diekstra et al., 2012), but the pathomechanism of how UNC13A is implicated remains to be elucidated.

EXPERIMENTAL PROCEDURES

Drosophila Stocks

The generation of human *UAS-TDP-43* constructs is described in Supplemental Experimental Procedures. Additional stocks used were *UAS-SpH*

(Miesenböck et al., 1998), *UAS-hELP3* (Miśkiewicz et al., 2011), *tbph*$^{\Delta 23}$, *tbph*$^{\Delta 142}$, *tbph*^{0} (Feiguin et al., 2009; Fiesel et al., 2010), *hdac6*^{ko} (Du et al., 2010), *w*^{1118}, *Elav-Gal4, D42-Gal4, nSyb-Gal4, Act-Gal4* and *y*^{1} *w*^{67c23} *P{EPgy2} HDAC6*^{EY09607} to overexpress HDAC6 (Bloomington Stock Center).

Microscopy

Larvae were dissected HL-3 and fixed in 4% formaldehyde and incubated at 1:100 with anti-BRP^{C} (NC82) or at 1:200 with anti-BRP^{N} (Fouquet et al., 2009), followed by 1:1,000 anti-mouse Alexa Flour 555 or anti-rabbit Alexa Flour 555 antibodies (Invitrogen). The mean intensity of BRP was measured per boutonic area using ImageJ in confocal images taken on a Nikon A1R confocal microscope using a 60× 1.35 numerical aperture (NA) oil lens and calculated following background subtraction. For PiMP, BRP^{C} dots were then continuously imaged for 200 frames at maximal speed in one single Z-optical section using a Leica SP5 II confocal microscope with a 63× 1.4 NA oil lens and at 44 nm pixel size, and the data were processed as described elsewhere (Munck et al., 2012). The surface areas of BRP^{C}-labeled objects parallel to the optical view (seen from the top) were manually traced using ImageJ. PiMP images are shown with contrast optimizing using the convolution filter in ImageJ, and electron microscopy was performed as described previously (Miśkiewicz et al., 2011). To quantify T-bar top size, we used serial-section electron microscopy and measured the top size in the "middle section" where the T-bar pedestal was broadest. For SpH imaging, motor neurons were stimulated at 60 Hz 50 AP in HL-3 with 2 mM $CaCl_2$ and imaged at 100 ms intervals using an Andor Clara camera on a Nikon FN1 microscope with 60× 1 NA W lens as described elsewhere (Miśkiewicz et al., 2011).

Electrophysiology

Excitatory junctional currents were recorded in HL-3 at 0.2 Hz or at 60 Hz as described previously (Miśkiewicz et al., 2011) and in the Supplemental Experimental Procedures.

RT-PCR

RNA was isolated using TRI Reagent (Sigma-Aldrich), and 1 μg of total RNA was used for oligodT-primed double-stranded cDNA synthesis (SuperScriptIII; Invitrogen). A total of 20 ng cDNA was used for *HDAC6*, *TDP43*, and *HDAC4* SYBR Green PCR Master mix (Applied Biosystems). Experiments were repeated three times and run in triplicate (nine repeats) on a Roche LC480. Data were normalized to *RP49*.

Biochemistry

Immunoprecipitation of BRP was performed as described elsewhere (Miśkiewicz et al., 2011) and in Supplemental Experimental Procedures. For deacetylation reactions, immunoprecipitated BRP (from ~300 heads) (Miśkiewicz et al., 2011) was incubated with 4 μg HDAC6 (Sigma-Aldrich) in acetylation buffer at 25°C for the times indicated, and acetylation was assessed using western blotting. Antibodies used were 1:500 anti-acetylated lysine (ac-K; rabbit, AB80178; Abcam), 1:1,000 anti-BRP^{D2} (Fouquet et al., 2009), 1:1,000 anti-BRP^{C} (Developmental Studies Hybridoma Bank), and 1:1,000 horseradish peroxidase-coupled secondary antibodies (Jackson ImmunoResearch). Blots were imaged using a digital imager, and the mean intensity of bands was measured and the background subtracted using ImageJ.

Fly Activity Assays

For negative geotaxis, 22-day-old flies were tested for the ability to climb 8 cm in 10 s. For activity measurements, 21-day-old male flies were monitored using the *Drosophila* activity monitor system (Trikinetics) (Gilestro, 2012). The average activity starting at 1 hr before the lights were turned on until 1 hr after they were turned on is reported; we call this average activity in this 2 hr interval the "morning peak."

Statistics

Data sets were tested for normality of the distribution. A multiple-comparison parametric test (ANOVA) was used when comparing multiple groups. Not-normally distributed data were analyzed using a nonparametric test (Kruskal-Wallis). Significance in comparison to controls was tested using Dunnett's test for normal distribution or Dunn's test for nonnormal distributions, and each group was also compared to the corresponding control with an unpaired t test. For genetic interactions, rescue groups were compared with corresponding mutants with an unpaired t test.

SUPPLEMENTAL INFORMATION

Supplemental Information includes Supplemental Experimental Procedures and three figures and can be found with this article online at http://dx.doi.org/10.1016/j.celrep.2014.05.051.

AUTHOR CONTRIBUTIONS

K.M., L.E.J., and P.V. designed the study and wrote the paper. Data were analyzed by K.M. (immunohistochemistry, TEM, and PiMP), L.E.J. (biochemistry, RT-PCR, and behavior), and P.V. (electrophysiology and SpH). K.M., L.E.J., W.M.Y., J.S., and P.V. performed experiments, and J.S.V., S.M., F.F., and B.D. provided reagents or tools.

ACKNOWLEDGMENTS

We thank B. De Strooper, J. De Wit, R. Goodchild, B. Hassan, W. Robberecht, and members of the Verstreken lab for comments and S. Sigrist (University of Berlin), C. Wang (NLM, Beijing), H. Bellen (BCM, Houston), A. Di Antonio (Washington University) the Bloomington Stock Center, and the Developmental Studies Hybridoma Bank for reagents. Support was provided by an ERC starting grant (260678), a GOA from the Research Fund KU Leuven, the Hercules Foundation, and VIB (Belgium) (to P.V.); FWO grants and an IUAP by BELSPO (to P.V. and B.D.); and the Inserm, the University of Lille 2, DN2M:Etat Région Nord/Pas-de-Calais (France) (to B.D.).

Received: December 23, 2013
Revised: April 18, 2014
Accepted: May 29, 2014
Published: June 26, 2014

REFERENCES

Ayala, Y.M., De Conti, L., Avendaño-Vázquez, S.E., Dhir, A., Romano, M., D'Ambrogio, A., Tollervey, J., Ule, J., Baralle, M., Buratti, E., and Baralle, F.E. (2011). TDP-43 regulates its mRNA levels through a negative feedback loop. EMBO J. *30*, 277–288.

Diekstra, F.P., van Vught, P.W.J., van Rheenen, W., Koppers, M., Pasterkamp, R.J., van Es, M.A., Schelhaas, H.J., de Visser, M., Robberecht, W., Van Damme, P., et al. (2012). UNC13A is a modifier of survival in amyotrophic lateral sclerosis. Neurobiol. Aging *33*, 630.e3–8.

Du, G., Liu, X., Chen, X., Song, M., Yan, Y., Jiao, R., and Wang, C. (2010). Drosophila Histone Deacetylase 6 Protects Dopaminergic Neurons against α-Synuclein Toxicity by Promoting Inclusion Formation *21*, 2128–2137.

Estes, P.S., Boehringer, A., Zwick, R., Tang, J.E., Grigsby, B., and Zarnescu, D.C. (2011). Wild-type and A315T mutant TDP-43 exert differential neurotoxicity in a Drosophila model of ALS. Hum. Mol. Genet. *20*, 2308–2321.

Feiguin, F., Godena, V.K., Romano, G., D'Ambrogio, A., Klima, R., and Baralle, F.E. (2009). Depletion of TDP-43 affects Drosophila motoneurons terminal synapsis and locomotive behavior. FEBS Lett. *583*, 1586–1592.

Fiesel, F.C., Voigt, A., Weber, S.S., Van den Haute, C., Waldenmaier, A., Görner, K., Walter, M., Anderson, M.L., Kern, J.V., Rasse, T.M., et al. (2010). Knockdown of transactive response DNA-binding protein (TDP-43) downregulates histone deacetylase 6. EMBO J. *29*, 209–221.

Fouquet, W., Owald, D., Wichmann, C., Mertel, S., Depner, H., Dyba, M., Hallermann, S., Kittel, R.J., Eimer, S., and Sigrist, S.J. (2009). Maturation of active zone assembly by Drosophila Bruchpilot. J. Cell Biol. *186*, 129–145.

Fukada, M., Hanai, A., Nakayama, A., Suzuki, T., Miyata, N., Rodriguiz, R.M., Wetsel, W.C., Yao, T.-P., and Kawaguchi, Y. (2012). Loss of deacetylation activity of Hdac6 affects emotional behavior in mice. PLoS ONE *7*, e30924.

Gilestro, G.F. (2012). Video tracking and analysis of sleep in Drosophila melanogaster. Nat. Protoc. *7*, 995–1007.

Hallermann, S., Kittel, R.J., Wichmann, C., Weyhersmüller, A., Fouquet, W., Mertel, S., Owald, D., Eimer, S., Depner, H., Schwärzel, M., et al. (2010a). Naked dense bodies provoke depression. J. Neurosci. *30*, 14340–14345.

Hallermann, S., Heckmann, M., and Kittel, R.J. (2010b). Mechanisms of short-term plasticity at neuromuscular active zones of Drosophila. HFSP J. *4*, 72–84.

Hubbert, C., Guardiola, A., Shao, R., Kawaguchi, Y., Ito, A., Nixon, A., Yoshida, M., Wang, X.-F., and Yao, T.-P. (2002). HDAC6 is a microtubule-associated deacetylase. Nature *417*, 455–458.

Khuong, T.M., Habets, R.L.P., Slabbaert, J.R., and Verstreken, P. (2010). WASP is activated by phosphatidylinositol-4,5-bisphosphate to restrict synapse growth in a pathway parallel to bone morphogenetic protein signaling. Proc. Natl. Acad. Sci. USA *107*, 17379–17384.

Kim, S.H., Shanware, N.P., Bowler, M.J., and Tibbetts, R.S. (2010). Amyotrophic lateral sclerosis-associated proteins TDP-43 and FUS/TLS function in a common biochemical complex to co-regulate HDAC6 mRNA. J. Biol. Chem. *285*, 34097–34105.

Kittel, R.J., Wichmann, C., Rasse, T.M., Fouquet, W., Schmidt, M., Schmid, A., Wagh, D.A., Pawlu, C., Kellner, R.R., Willig, K.I., et al. (2006). Bruchpilot promotes active zone assembly, Ca2+ channel clustering, and vesicle release. Science *312*, 1051–1054.

Kovacs, J.J., Murphy, P.J.M., Gaillard, S., Zhao, X., Wu, J.-T., Nicchitta, C.V., Yoshida, M., Toft, D.O., Pratt, W.B., and Yao, T.-P. (2005). HDAC6 regulates Hsp90 acetylation and chaperone-dependent activation of glucocorticoid receptor. Mol. Cell *18*, 601–607.

Matkovic, T., Siebert, M., Knoche, E., Depner, H., Mertel, S., Owald, D., Schmidt, M., Thomas, U., Sickmann, A., Kamin, D., et al. (2013). The Bruchpilot cytomatrix determines the size of the readily releasable pool of synaptic vesicles. J. Cell Biol. *202*, 667–683.

Miesenböck, G., De Angelis, D.A., and Rothman, J.E. (1998). Visualizing secretion and synaptic transmission with pH-sensitive green fluorescent proteins. Nature *394*, 192–195.

Miśkiewicz, K., Jose, L.E., Bento-Abreu, A., Fislage, M., Taes, I., Kasprowicz, J., Swerts, J., Sigrist, S., Versées, W., Robberecht, W., and Verstreken, P. (2011). ELP3 controls active zone morphology by acetylating the ELKS family member Bruchpilot. Neuron *72*, 776–788.

Mukherjee, K., Yang, X., Gerber, S.H., Kwon, H.-B., Ho, A., Castillo, P.E., Liu, X., and Südhof, T.C. (2010). Piccolo and bassoon maintain synaptic vesicle clustering without directly participating in vesicle exocytosis. Proc. Natl. Acad. Sci. USA *107*, 6504–6509.

Munck, S., Miskiewicz, K., Sannerud, R., Menchon, S.A., Jose, L., Heintzmann, R., Verstreken, P., and Annaert, W. (2012). Sub-diffraction imaging on standard microscopes through photobleaching microscopy with non-linear processing. J. Cell Sci. *125*, 2257–2266.

Ohtsuka, T., Takao-Rikitsu, E., Inoue, E., Inoue, M., Takeuchi, M., Matsubara, K., Deguchi-Tawarada, M., Satoh, K., Morimoto, K., Nakanishi, H., and Takai, Y. (2002). Cast: a novel protein of the cytomatrix at the active zone of synapses that forms a ternary complex with RIM1 and munc13-1. J. Cell Biol. *158*, 577–590.

Reed, N.A., Cai, D., Blasius, T.L., Jih, G.T., Meyhofer, E., Gaertig, J., and Verhey, K.J. (2006). Microtubule acetylation promotes kinesin-1 binding and transport. Curr. Biol. *16*, 2166–2172.

Siksou, L., Rostaing, P., Lechaire, J.-P., Boudier, T., Ohtsuka, T., Fejtová, A., Kao, H.-T., Greengard, P., Gundelfinger, E.D., Triller, A., and Marty, S. (2007). Three-dimensional architecture of presynaptic terminal cytomatrix. J. Neurosci. *27*, 6868–6877.

Simpson, C.L., Lemmens, R., Miskiewicz, K., Broom, W.J., Hansen, V.K., van Vught, P.W.J., Landers, J.E., Sapp, P., Van Den Bosch, L., Knight, J., et al. (2009). Variants of the elongator protein 3 (ELP3) gene are associated with motor neuron degeneration. Hum. Mol. Genet. *18*, 472–481.

Voigt, A., Herholz, D., Fiesel, F.C., Kaur, K., Müller, D., Karsten, P., Weber, S.S., Kahle, P.J., Marquardt, T., and Schulz, J.B. (2010). TDP-43-mediated neuron loss in vivo requires RNA-binding activity. PLoS ONE *5*, e12247.

Wagh, D.A., Rasse, T.M., Asan, E., Hofbauer, A., Schwenkert, I., Dürrbeck, H., Buchner, S., Dabauvalle, M.C., Schmidt, M., Qin, G., et al. (2006). Bruchpilot, a protein with homology to ELKS/CAST, is required for structural integrity and function of synaptic active zones in Drosophila. Neuron *49*, 833–844.

Zhang, X., Yuan, Z., Zhang, Y., Yong, S., Salas-Burgos, A., Koomen, J., Olashaw, N., Parsons, J.T., Yang, X.-J., Dent, S.R., et al. (2007). HDAC6 modulates cell motility by altering the acetylation level of cortactin. Mol. Cell *27*, 197–213.